

Avalanche dynamics in a deposition model with "sliding"

Z. Cheng and S. Redner

Center for Polymer Studies and Department of Physics, Boston University, Boston, Massachusetts 02215

P. Meakin

Central Research and Development Department, E.I. DuPont de Nemours and Company, Wilmington, Delaware 19880-0356

F. Family

Department of Physics, Emory University, Atlanta, Georgia 30322

(Received 12 April 1989)

We introduce a simple model of "avalanches" in which there is continuous deposition of mass on a "tilted" substrate, with avalanches occurring whenever the mass at a given site reaches a preassigned threshold value h_c . The avalanche is defined to sweep away all mass which is downhill from the initiation event. Basic dynamical features are studied, including the distribution of avalanche sizes and the time intervals between avalanches. For a one-dimensional "slope" of length L , the average avalanche size is found to scale as L^{1-1/h_c} , and in the continuum limit the averaged steady-state mass distribution a distance x from the top of the slope scales as x^{-1/h_c} . Qualitatively similar results are found for avalanches on a two-dimensional substrate. Contrasts between the present avalanche model and models of self-organized criticality are discussed.

I. INTRODUCTION

In this paper, we investigate the statistical properties of a simple "avalanche" model in which there is a continuous deposition of mass on a "tilted" substrate, with avalanches occurring whenever the mass at given site reaches a preassigned threshold value. In an avalanche, mass is defined as falling along a preferred direction which we consider as being imposed by an external field, such as gravity, and in the process coalesces with and removes all other mass that it contacts. Our model may mimic processes such as the falling off of water droplets on a thread, e.g., dew on a cobweb, or the flow of water on an inclined plane, e.g., rain on a window pane, or perhaps even real snow avalanches. The example of rain on a window pane appears to amenable to simple, yet quantitative experimental studies.

In addition to the potential connection with avalanche phenomena, we are also motivated by the "sandpile" models of self-organized criticality introduced by Bak and co-workers,^{1,2} which have generated considerable recent interest both theoretically^{3,4} and experimentally.⁵⁻⁷ Our avalanche model has several features in common with the sandpile models. There is a continuous input of mass into the system, with transport being initiated whenever the threshold for flow is exceeded locally. In the avalanche model, however, the mass transport after threshold has been attained has a catastrophic nature, as the avalanche ends only when the boundary of the system is reached. This feature strongly contrasts with the dissipation mechanism in the sandpile models. Due to this dissipation, the sandpile model naturally evolves to a self-organized critical state in which many dynamical quantities exhibit power-law correlations.¹⁻⁴ However,

the connection between the sandpile model and potential experimental realizations has yet to be fully realized.⁵⁻⁷ Our model appears to provide a better physical picture for certain types of transport in open systems, such as water droplets running down a window pane. Our goal is to explore the dynamical behavior of the avalanche model, and perhaps to gain general insights about generic models of open systems.

We have formulated both a lattice and an off-lattice version of an avalanche model incorporating (i) droplet deposition, (ii) droplet growth and coalescence, and (iii) ensuing avalanche. The first two features have already been studied extensively in a wide variety of contexts such as the growth of thin films,^{8,9} the growth of breath figures,^{10,11} and heterogeneous nucleation.^{12,13} The possibility of allowing for avalanching allows the system to achieve a steady state in which there is a fluctuating transport of mass out of the end of the system. The behavior of this mass flow is the main focus of this paper.

In the lattice version of the avalanche model, unit masses are sequentially deposited at random on a d -dimensional substrate of linear dimension L . When the mass at any lattice site reaches a threshold value h_c an avalanche begins in which this critical mass nucleus slides "downhill" and collects with it any mass which it contacts, either downstream or laterally, as illustrated in Fig. 1. In the off-lattice model, there is sequential, random deposition of D -dimensional hyperspherical droplets of diameter d_0 on the substrate. When two droplets of radii r_1 and r_2 touch or overlap, they coalesce into a larger droplet of radius $r = (r_1^D + r_2^D)^{1/D}$, whose location is at the center of mass of the two original droplets. If this newly created droplet overlaps other droplet(s), coalescence continues until no overlaps remain. When

the droplet mass reaches a threshold value h_c , it commences sliding down the substrate, still continuing to coalesce with other droplets in its path according to the mechanism just outlined. In our simulations of the avalanche model in two dimensions, periodic boundary conditions in the lateral direction are imposed.

We are interested in the statistical properties of the avalanches and in the nature of the steady-state mass dis-

tribution on the substrate. In this work, we will primarily focus on two characteristic properties of avalanches. These are, $P(t)$ which is the distribution of times between successive avalanches, and $R(m)$, the distribution of avalanche sizes. The former quantity coincides with the mass added between avalanches, if one mass is added to the system per unit time and if the avalanche propagation time is neglected compared to the time between mass deposition events. For both the lattice and off-lattice versions of the model, we find that these dynamical quantities obey simple scaling laws. However, the spatio-temporal correlations of the ensuing steady state are not generally of a long-range nature, i.e., this steady state does not appear to lie within the universality class of self-organized criticality.

For a one-dimensional substrate, we have calculated the steady-state properties and the temporal correlations of the avalanches. We have also studied the conditions for the initiation of the first avalanche in the system. In addition to analytical calculations, we have performed extensive numerical simulations of this avalanche process for both the lattice and continuum version of the model for one- and two-dimensional substrates. In the simulations of the lattice model, we injected between 1.5×10^9 and 7.5×10^9 particles in one dimension, and between 5×10^7 and 7.5×10^9 particles in two dimensions in order to study steady-state properties. For the continuum model, the number of particles added was typically one order of magnitude less than in the lattice models. These simulations required a total of approximately 600 h of CPU time on an IBM 3090 computer.

In Sec. II of this paper, we begin by giving a simple probabilistic derivation for when the first avalanche is expected to occur on a one-dimensional substrate. In Sec. III, we discuss the nature of the steady state in one dimension. For the case of the threshold $h_c = 2$ the steady state is found by a direct solution of the master equations that summarize the occupancy probability on the substrate. In the limit of $h_c \rightarrow \infty$, we present a complementary continuum approach from which we can derive the steady-state avalanche properties, as well as the spatial distribution of mass remaining on the substrate. In Sec. IV we present extensive simulation results for avalanches on two-dimensional substrates. Finally, in Sec. V we give a brief discussion of our results.

II. AVALANCHE INITIATION

We first determine the condition necessary for the occurrence of the initial avalanche for a one-dimensional lattice, as mass builds up on an initially empty system of length L . For the first avalanche to occur, it is necessary that h_c particles land on the same lattice site. This event can be expected to occur on a system of length L when the probability of the event is of the order of $1/L$. Using the Poisson distribution for the occupancies at each site, we therefore have

$$\frac{\langle h \rangle^{h_c}}{h_c!} e^{-\langle h \rangle} \sim \frac{1}{L}, \quad (1)$$

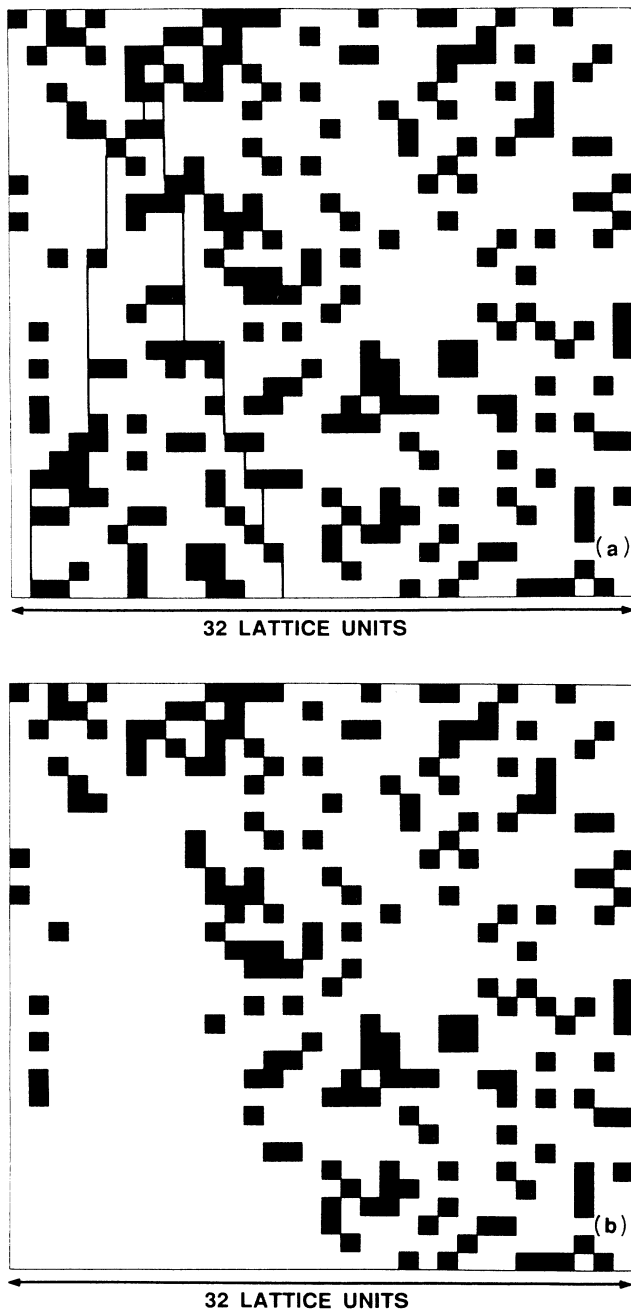


FIG. 1. Illustration of the discrete version of the avalanche model on a 32×32 substrate for $h_c = 3$. The system is shown (a) just before and (b) just after the avalanche. For this system size, the wedge-shaped cleared region is apparent.

where $\langle h \rangle$ is the average mass at each lattice site. As long as h_c is finite, this consideration leads to the first avalanche occurring when the mass deposited on the substrate is of the order of

$$M_0 \sim \left(\frac{h_c}{e} \right) L^{1-1/h_c}, \quad (2)$$

as $L \rightarrow \infty$.

A similar argument can be given to obtain the probability that the first avalanche occurs when m masses have been injected into the system. Before any avalanche has occurred, m coincides with the time t , and we may therefore use these two quantities interchangeably when referring to the properties of the first avalanche. To find the probability of the first avalanche, we first require the probability that there is no coincidence of order h_c when the m^{th} particle is injected. When this m^{th} particle is injected, the probability that $h_c - 1$ particles are on the same site is approximately equal to, from the Poisson distribution,

$$c_m \simeq \frac{\langle h \rangle^{h_c-1}}{(h_c-1)!}, \quad (3)$$

where we now define $\langle h \rangle = m/L = t/L$. In this expression, we have assumed that m is sufficiently small that the Poissonian exponential factor can be approximated by unity. Consequently, the probability that there are no coincidences of order h_c when the first m particles have been injected, $\mathcal{P}(m)$, is given by

$$\mathcal{P}(m) = \prod_{n=1}^m (1 - c_n), \quad (4a)$$

and expanding the product to lowest order leads to

$$\mathcal{P}(m) \sim \exp \left[- \sum_{n=1}^m c_n \right] \sim \exp \left[- \frac{L \langle h \rangle^{h_c}}{h_c!} \right]. \quad (4b)$$

Finally, the probability that there is a coincidence of order h_c when m particles have been added, or equivalently, at time t , is simply equal to $-d\mathcal{P}(t)/dt$. Thus we find for the distribution of times between successive avalanches

$$P(t) \simeq \frac{\langle h \rangle^{h_c-1}}{(h_c-1)!} \exp \left[- \frac{L \langle h \rangle^{h_c}}{h_c!} \right]. \quad (5)$$

Since the location of the initial avalanche is uniformly distributed on the substrate, we also expect that the size distribution of the initial avalanche will be uniform until a characteristic size which is of the order of M_0 , beyond which the distribution is exponentially cut off.

These features are observed in our simulation data shown in Fig. 2. In addition to the distribution for first avalanche times and sizes, we have also considered the moments of these distributions. Specifically, the average time until the first avalanche is defined by

$$\tau = \sum_t t P(t), \quad (6a)$$

and the average size of the first avalanche by

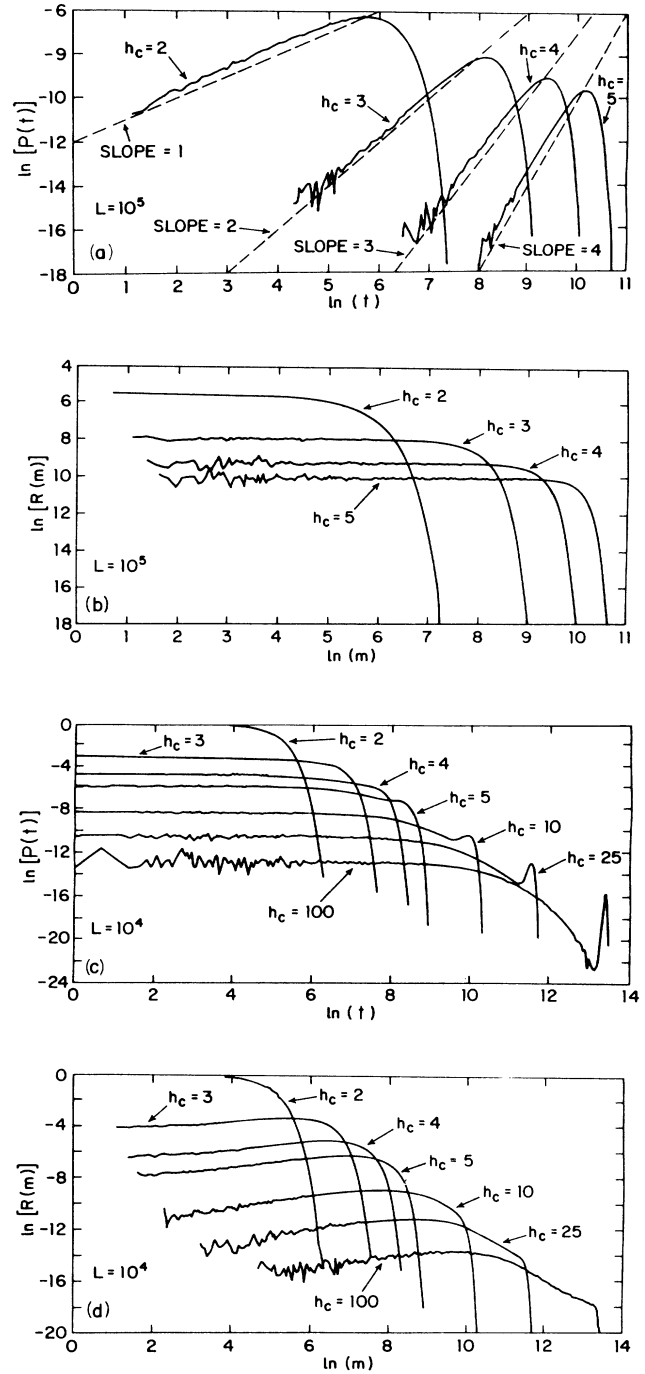


FIG. 2. Numerical simulations of the discrete avalanche model in one dimension for various values of h_c . Shown in (a) is the distribution of times until the first avalanche (or equivalently, the mass added before the first avalanche) $P(t)$, and in (b) the size distribution of the initial avalanche $R(m)$, both for an interval of length $L = 10^5$. In (c) and (d), the respective steady-state distributions for these two quantities are shown based on simulations on an interval with $L = 10^4$. In (c), note the peak in $P(t)$ at large times for large values of h_c . This peak corresponds to the avalanches that occur after the slope is swept clean, and it therefore coincides with the distribution of times required to initiate the first avalanche.

$$\mathcal{M} = \sum_m mR(m). \quad (6b)$$

By using Eq. (5) for $P(t)$, we find

$$\tau \sim L^\alpha, \quad (7a)$$

with $\alpha = 1 - 1/h_c$. On the other hand, from the numerical data of Fig. 2, it also appears that \mathcal{M} can be well represented by the power-law relation

$$\mathcal{M} \sim L^{\alpha'}. \quad (7b)$$

From plotting the L dependence of the numerical estimates for α and α' on a double logarithmic scale, we estimate effective L -dependent values for the exponents α and α' , which we then extrapolate to the $L \rightarrow \infty$ limit (Fig. 3). The data suggest that the asymptotic $L \rightarrow \infty$ values of both these exponents are

$$\alpha = \alpha' = 1 - 1/h_c, \quad (8)$$

in agreement with our elementary probabilistic treatment. In the off-lattice case, an avalanche is initiated whenever a mass h_c has been deposited in an interval of length $h_c^{1/D}$. This is equivalent to the lattice case with L playing the role of $h_c^{1/D}$.

III. STEADY-STATE PROPERTIES

A. Mass threshold $h_c = 2$

We now present an analytic solution for the distribution of avalanche sizes and time intervals between

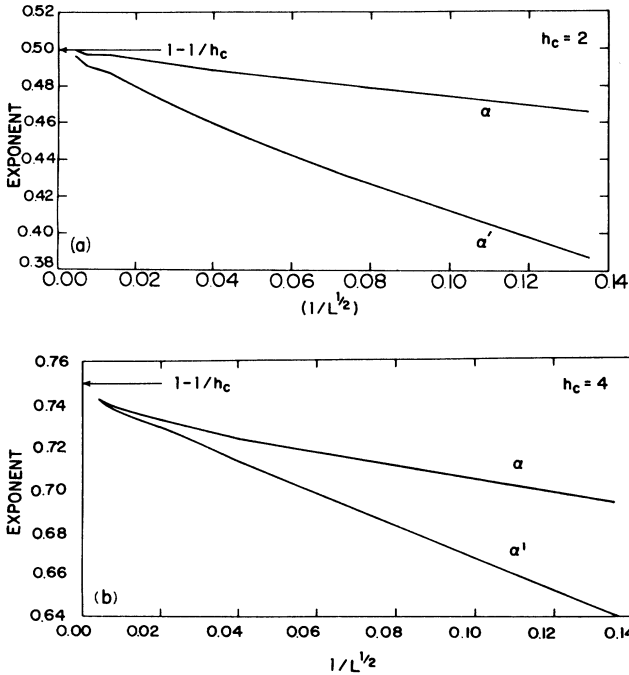


FIG. 3. Dependence of the effective exponents $\alpha(L)$ and $\alpha'(L)$. Here $\alpha(L)$ is defined as $\{\ln[P(t, L_2)] - \ln[P(t, L_1)]\} / (\ln L_2 - \ln L_1)$ with $L = \sqrt{L_1 L_2}$, and $\alpha'(L)$ is defined similarly. Shown are the cases (a) $h_c = 2$ and (b) $h_c = 4$.

avalanches in the steady state when the threshold for avalanche initiation h_c equals 2. This solution hinges on the fact that the evolution of the system depends only on whether a mass added to the system falls on an empty site or a previously occupied site. If the particle lands on an already occupied site an avalanche must occur, while if the particle lands on an empty site there is no subsequent avalanche event. In addition to the intrinsic interest of this solution, it also serves as a useful check on the numerical simulations.

We begin by calculating the probability that there exist j particles on an interval of length L at the N^{th} time step, $p_N(j)$. This quantity obeys the recursion relation

$$p_N(j) = \left(1 - \frac{j}{L}\right) p_{N-1}(j-1) + \sum_{j'=j+1}^L \frac{1}{L} p_{N-1}(j'). \quad (9)$$

The first term accounts for the possibility that an interval containing $j-1$ particles can accommodate an additional particle without the occurrence of an avalanche, while the second term accounts for the ways in which the addition of a single particle to an interval containing j' particles can lead to an avalanche with j particles being left behind (Fig. 4).

Equation (9) can be rewritten in the matrix form $\mathcal{P}_N = \mathcal{M} \cdot \mathcal{P}_{N-1}$, where \mathcal{P}_N is the column vector whose j^{th} component is $p_N(j)$, and \mathcal{M} is the $(L+1) \times (L+1)$ matrix

$$\begin{pmatrix} 0 & \frac{1}{L} & \cdots & \frac{1}{L} \\ 1 & 0 & \frac{1}{L} & \vdots \\ 0 & \frac{L-1}{L} & 0 & \ddots \\ \vdots & & \frac{L-2}{L} & \ddots \\ & & & \ddots & \frac{1}{L} \\ & & & \cdots & \frac{1}{L} & 0 \end{pmatrix}. \quad (10)$$

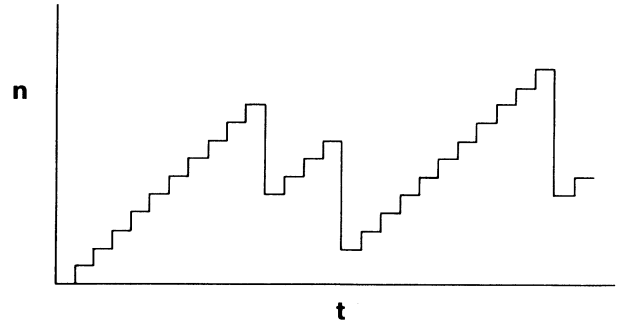


FIG. 4. Illustration of the temporal evolution of the number of particles in the system, n . Single-particle addition corresponds to an upward step of unit length. For a system containing n particles such a step occurs with probability $1 - n/L$. An avalanche corresponds to a downward step which can end at any point $n' < n$; the probability of each of these n possibilities is $1/L$.

From this, we find that $p_N(j)$ has the steady-state solution

$$p_\infty(j) = \frac{L!(j+1)}{(L-j)!(L+1)^{j+1}}. \quad (11)$$

Using Stirling's approximation, the steady-state mass on the interval is peaked at a value that scales as \sqrt{L} , i.e., as L^{1-1/h_c} with $h_c=2$.

From this distribution of steady-state occupancies, we can now determine the distribution of avalanche sizes and the time between avalanches. For this purpose, note that there is a unique location for the insertion of a particle in an interval containing $n > m-1$ particles that leads to an avalanche of mass m . Consequently, the steady-state distribution of avalanche sizes can be written as

$$R(m+1) = \frac{\sum_{n=m}^L [p_\infty(n)/L]}{\sum_{m=1}^L \sum_{n=m}^L [p_\infty(n)/L]}, \quad m=1,2,\dots,L. \quad (12a)$$

By exploiting Eq. (9), the sum over $p_\infty(n)$ can be eliminated to yield the closed-form expression

$$R(m+1) = \frac{1}{\langle \mathcal{M} \rangle} \frac{L+1}{m+1} p_\infty(m). \quad (12b)$$

where $\langle \mathcal{M} \rangle$ is the average size of the avalanches in the steady state.

By a very similar line of reasoning, the distribution of time intervals between avalanches, or equivalently, the mass added between avalanches, can be formally written as $P(t) = \mathcal{P}(t) / \sum_t \mathcal{P}(t)$, with

$$\begin{aligned} \mathcal{P}(t) = & \sum_{n=1}^{L-t+2} \sum_{l=n}^L \frac{p_\infty(l)}{L} \frac{L-n+1}{L} \frac{L-n}{L} \\ & \times \dots \times \frac{L-n-t+3}{L} \frac{n+t-2}{L}. \end{aligned} \quad (13a)$$

The factors in the product express the probability that in an interval which contains l masses, no subsequent avalanche occurs for the next t time units. Since one mass is added at each time step, t and m can again be used interchangeably in Eqs. (12) and (13). Now appealing to Eq. (9), $P(t)$ can be reduced to

$$\begin{aligned} P(t) \propto & \left[\frac{L+1}{L} \right]^t \left[\left[1 + \frac{3}{L} + \frac{2}{L^2} \right] R(t) \right. \\ & \left. - \frac{L!(2L+t+1)}{(L+1)^L L^2 \langle \mathcal{M} \rangle} \sum_{n=0}^{L-t+1} \frac{(L+1)^n}{n!} \right] \\ \rightarrow & R(t) + \mathcal{O} \left[\frac{1}{L} \right], \quad t=1,2,\dots,L+1, \end{aligned} \quad (13b)$$

where the second relation continues to hold for the case $t=m=1$ if we continue to define $R(1)$ via Eq. (12b). The basic qualitative features of these expressions for $R(m)$ and $P(t)$ is that they are similar in behavior to $p_\infty(m)$.

They are relatively featureless for $m < \sqrt{L}$, and are exponentially cut off for $m > \sqrt{L}$. Our simulation results for $R(m)$ and $P(t)$ are shown in Figs. 2(c) and 2(d) for various values of h_c . For $h_c=2$, the simulation data are in excellent agreement with Eqs. (12) and (13).

B. Large threshold

For large values of h_c , numerical simulations indicate that a steady state is reached relatively quickly, so that many properties of the steady state and the initial avalanche are fairly similar. Thus the exponent values $\alpha=\alpha'=1-1/h_c$ also appear to describe the scaling of the average avalanche size and the average time interval between avalanches in the steady state. For large h_c , the distribution of avalanche sizes is still quite flat for sizes less than a characteristic size. However, for the distribution of avalanche intervals the flat region is followed by a pronounced minimum and then a sharp peak at the largest possible times [Figs. 2(c) and (d)].

This striking behavior can be understood from the peculiar evolution of the system in the large h_c limit. Starting with an empty substrate, there is a long quiescent period during which mass builds up to a point that is close to the threshold value at each site. When the first avalanche finally does occur, the upstream portion of the system is still close to the avalanche threshold. Consequently this portion of the substrate is highly susceptible to additional avalanching soon after the initial event. This suggests that there will follow a relatively short "burst" of avalanche activity in which the initiation point of the avalanche moves upstream through the near-threshold portion of the system at each successive event. This burst terminates when an avalanche occurs at the top of the slope, thereby sweeping the slope clean. The large-time peak in the steady-state distribution $P(t)$ originates from the long time needed to generate an avalanche after the slope has been swept clean. The location of this peak quantitatively coincides with the distribution $P(t)$ associated with the first avalanche.

We now develop this physical picture for the dynamics in the large h_c limit in order to provide quantitative predictions for steady-state properties. Before the first avalanche occurs, the mass at each site obeys a Gaussian distribution $p(h)$ whose average value $\langle h \rangle$ increases linearly in time, and whose width is of the order of $\sqrt{\langle h \rangle}$. The maximum mass at any site h_{\max} is determined by the condition $\int_{h_{\max}}^{\infty} p(h) dh = 1/L$. When h_{\max} reaches h_c the first avalanche occurs. From the integral condition for h_{\max} , we thereby find that the first avalanche occurs at a time $\tau_1/L \equiv T_L \sim h_c - \sqrt{2h_c \ln L}$, and at a random location on the interval.

Since the upstream portion of the system is nearly full at this time, the second avalanche almost surely occurs upstream of the first avalanche. The length of this upstream segment L' , will typically be equal to $L/2$. Consequently, the typical time for the occurrence of the second avalanche τ_2/L coincides with the time required for the first avalanche in a system of length L' , i.e., $\tau_2/L = T_{L'}$. Following this argument, the time delay un-

til the i^{th} avalanche is $\tau_i/L \sim T_{i-1}$, where the typical distance of the i^{th} avalanche from the top of the slope is $l_i \sim L/2^i$, and the mass carried by this avalanche is $m_i \sim l_i h_c$. Eventually an avalanche occurs at the top of the slope after a time delay, $\tau_{\text{renewal}}/L \sim h_c$, after which the avalanche sequence starts over again.

From this picture of avalanche events, the density profile a distance x from the top of the slope, $h(x)$, averaged over all realizations of the system will be of the order of one-half the time needed for an avalanche to occur at this position. Therefore,

$$h(x) \sim \frac{h_c}{2} - \left[\frac{h_c}{2} \ln x \right]^{1/2}. \quad (14)$$

In addition, the typical size reduction of successive avalanches by a factor of 2 suggests that the number of avalanches in a renewal cycle is of the order of $\ln L$. Consequently, the average avalanche mass is given by

$$M_L \sim \frac{L h_c}{\ln L}. \quad (15)$$

These two formulas suggest that there is a crossover from the large- h_c limit to the large- L limit when $h_c \sim \ln L$. In the large L limit, the density profile on the substrate can be viewed as a continuous function. This forms the basis for a continuum approximation which leads to detailed results about the statistics of avalanches. This approach will be treated in III C.

C. Finite deposition rate model for the thermodynamic limit

For arbitrary but large values of h_c and for large L , the average density profile on the substrate becomes a smoothly varying function of position. To discuss avalanche statistics, it proves very useful to introduce a variant of our original avalanche model in which each lattice site may be occupied by an additional particle with probability p at each time step. Since mass is deposited at a rate p per site, then pL particles will be added to the substrate in a unit time interval. In the limit where p approaches 0 as $1/L$, the behavior of this continuum “finite- p ” model approaches that of the original avalanche model in that one mass is added per unit time interval. However, this finite- p model lends itself naturally to a continuum description that facilitates the solution in the large L limit.

For the finite- p model, let $P_L(t)$ be the probability distribution for a time interval t between successive avalanches, where we now make explicit the fact that this distribution depends on the system length L . Furthermore, denote by $\{t_i\}$ the sequence of time intervals between successive avalanches in a system of length L . This coincides with the sequence of time intervals for avalanches that pass through column L of an infinite system. We now construct a master equation for $P_L(t)$ by relating the time interval sequence $\{T_i\}$ associated with avalanches that pass through column $L+1$, to the time sequence $\{t_i\} \subset \{T_i\}$, associated with avalanches that pass through column L of the same interval (Fig. 5). The solution to this master equation provides information about the dis-

tribution of time intervals between avalanches.

Consider the difference sequence $\{\tau_i\} = \{T_i\} - \{t_i\}$ which delineates the temporal occurrences of avalanches which *begin* at column $L=1$. Since each T_j belongs to some interval $[t_i, t_{i+1}]$, and since at every t_i the mass on column $L+1$ is reset to zero, the statistics of T_j depends only on the enclosing interval $[t_i, t_{i+1}]$. For large L , the probability of having more than one T_j in a time interval $[t_i, t_{i+1}]$ is small and therefore we make the “one-avalanche” approximation (Fig. 5) in which at most one T_j occurs in any interval $[t_i, t_{i+1}]$. Within this approximation, the master equation that relates $P_L(t) = \text{Prob}(t = t_{i+1} - t_i)$ to $P_{L+1}(t) = \text{Prob}(t = T_{i+1} - T_i)$ reduces to

$$P_{L+1}(t) = P_L(t) \sum_{t'=t}^{\infty} P_1(t') + \frac{1}{2} \sum_{t'=1}^{\infty} P_L(t+t') P_1(t') + \frac{1}{2} P_1(t) \sum_{t'=t+1}^{\infty} P_L(t'). \quad (16)$$

The first term on the right-hand side is the contribution from a time interval $[t_i, t_{i+1}]$ of duration t in which no avalanche occurs on the $(L+1)$ th column, while the last two terms correspond to the ways in which the time interval $[t_i, t_{i+1}]$ of duration longer than t can be split into two subintervals, with one of duration equal to t , by the occurrence of an avalanche on the $(L+1)$ th column. These equations are the discrete rate equations for the “fragmentation” of the time interval $t_{i+1} - t_i$ due to the introduction of a new avalanche event within the interval, in which L is the analog of the time and t the analog of the fragment sizes.¹⁴

We now take the continuum limit by letting $p \rightarrow 0$ and also rescaling t by a factor of p , i.e., the deposition rate is now L particles in a unit time interval. With this convention, $P_1(t)$ becomes the Poisson distribution $P_1(t) = t^{h_c-1} e^{-t}/(h_c-1)!$. Thus Eq. (16) can be recast as

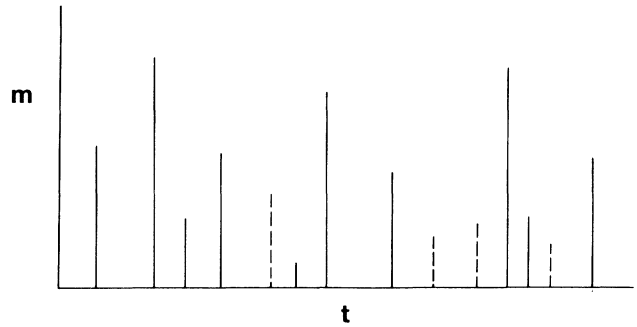


FIG. 5. A schematic time sequence of avalanches for an interval of length l (solid peaks), and the additional avalanches that begin at column $l+1$ (dashed peaks). The “one-avalanche” approximation is based on assuming that no more than one small avalanche appears between large avalanches.

$$\begin{aligned} \frac{\partial P_L(t)}{\partial L} &= -P_L(t) \int_0^t P_1(t') dt' \\ &+ \frac{1}{2} \int_0^\infty P_L(t'+t) P_1(t') dt' \\ &+ \frac{1}{2} P_1(t) \int_t^\infty P_L(t') dt'. \end{aligned} \quad (17)$$

Since the typical time between avalanches goes to zero as the size of the system increases, we anticipate that the asymptotic behavior of $P_L(t)$ can be written in the scaling form¹⁵

$$P_L(t) = T_L^{-1} \phi(t/T_L). \quad (18)$$

Here T_L is the typical time between avalanches on an interval of length L , and the exponent value -1 is required by the normalization of the total probability. Substituting this scaling form into the rate equations and making use of the fact that as $L \rightarrow \infty$, $e^{-x/T_L} \rightarrow 1$ with $x \equiv t/T_L$, the dependence on x and T_L in Eq. (17) can be separated into two equations:

$$\begin{aligned} -T_L^{-2} \frac{dT_L}{dL} &= \frac{T_L^{h_c-1}}{(h_c-1)!} \omega, \\ [\phi(x) + x\phi'(x)]\omega &= -\frac{\phi(x)x^{h_c}}{h_c} + \frac{x^{h_c-1}}{2} \int_x^\infty \phi(y) dy \\ &+ \frac{1}{2} \int_0^\infty y^{h_c-1} \phi(x+y) dy. \end{aligned} \quad (19)$$

The first equation can be immediately solved to yield for the typical time between avalanches:

$$T_L = (L/h_c!)^{-1/h_c} (\omega h_c^2)^{-1/h_c}. \quad (20)$$

Since the average mass residing on the L^{th} column is proportional to T_L , Eq. (20) also predicts that there is a power-law density profile as a function of distance from the beginning of the interval, with a characteristic exponent $-1/h_c$. A related quantity, which can be found by this reasoning is the distribution of positions at which an avalanche occurs, $Q(x)$. Since $T_L^{-1} \sim \int^L Q(x) dx$, we conclude that $Q(x) \sim x^{-1+1/h_c}$ for large x .

At this stage, we convert the integrodifferential equation for the scaling function $\phi(x)$ to a recursion relation between the moments $m_k \equiv \int_0^\infty x^k \phi(x) dx$. Thus by multiplying the second half of Eq. (19) by x^k and integrating over all x , we find

$$\omega k m_k = m_{k+h_c} \left[\frac{1}{h_c} - \frac{1}{2(k+h_c)} - \frac{\beta(k+1, h_c)}{2} \right] \quad \text{for } k \geq 1. \quad (21)$$

where $\beta(n, m)$ is the β function. In both the limits $x \rightarrow 0$ and $x \rightarrow \infty$, these recursion relations can be solved to yield the asymptotic behavior of the moments. Then by inverting the Mellin transform, we find the following asymptotic forms for $\phi(x)$:

$$\phi(x) = \begin{cases} m_{h_c-1} + \text{const} \times x, & x \ll 1 \\ (x^{h_c-1}/h_c^3) \exp(-x^{h_c}/\omega h_c^2), & x \gg 1 \end{cases}. \quad (22)$$

Substituting Eqs. (21) and (22) into the definition (18) for $P_L(t)$, we find

$$P_L(t) \propto \begin{cases} L^{1/h_c}, & \text{small time} \\ L^{-1/h_c} t^{h_c-1} \exp(-Lt^{h_c}/h_c!), & \text{large time} \end{cases}. \quad (23)$$

Here the crossover between small and large times is determined by comparing t with the quantity $(h_c!/\omega h_c^2 L)^{1/h_c}$. For large times, Eq. (23) coincides with the time interval distribution for the first avalanche given in Eq. (5) when the time t is identified with $\langle h \rangle$ in (5). On the other hand, for small times, Eq. (22) approaches a constant [Fig. 2(c)], while Eq. (5) has a power-law time dependence t^{h_c-1} [Fig. 2(a)].

D. Autocorrelation functions for mass transport

We now study the autocorrelation functions associated with the mass transport to quantify the fluctuations in the mass flow through the system. For this purpose, we define the autocorrelation function for the mass contained in the interval

$$c_{\text{mass}}(t) \equiv \langle n(t')n(t'+t) \rangle - \langle n(t') \rangle^2, \quad (24)$$

where $n(t)$ is the total mass in the system at time t , and the angle brackets denote a time average over t' . Here we define the time so that the deposition rate is one particle per unit time interval. For the particular case $h_c = 2$, we can exploit the matrix formulation for the evolution of the system upon single-particle addition, Eq. (10), to formally write the autocorrelation function as

$$c_{\text{mass}}(t) = (0, 1, 2, \dots, L) M^t \begin{bmatrix} 0 \times p_\infty(0) \\ 1 \times p_\infty(1) \\ L \times p_\infty(L) \end{bmatrix} - \langle n(t) \rangle^2. \quad (25)$$

Since the net mass leaving the system at time t is simply $n(t+1) - n(t) - 1$, the autocorrelation of the flux $c_{\text{flux}}(t)$ is given by

$$c_{\text{flux}}(t) = 2c_{\text{mass}}(t) - c_{\text{mass}}(t-1) - c_{\text{mass}}(t+1). \quad (26)$$

By diagonalizing the matrix M for intervals up to $L = 400$ and also by direct simulation of the autocorrelation function for an interval of length 25,000, we obtain identical results, which are shown in Fig. 6(a). At short times, there is an anticorrelation of the flux which merely reflects the fact that immediately after one avalanche has occurred, there will be a finite time delay until the next avalanche. At long times, the correlation function is flat, indicative of no long-term memory effects. This behavior continues to hold for small values of $h_c > 2$ [Fig. 6(b)]. On the other hand, for large h_c there is an oscillation in

the correlation function with a periodicity that coincides with the “renewal” time, i.e., the time for the slope to be swept clean [Fig. 6(c)].

In two dimensions, we observe qualitatively similar behavior, except for the oscillations associated with the

large h_c limit. The absence of the oscillations stems from the lack of a well-defined renewal event. In both one and two dimensions, it appears that the correlation function decays rather quickly; there does not appear to be any evidence for power-law behavior.

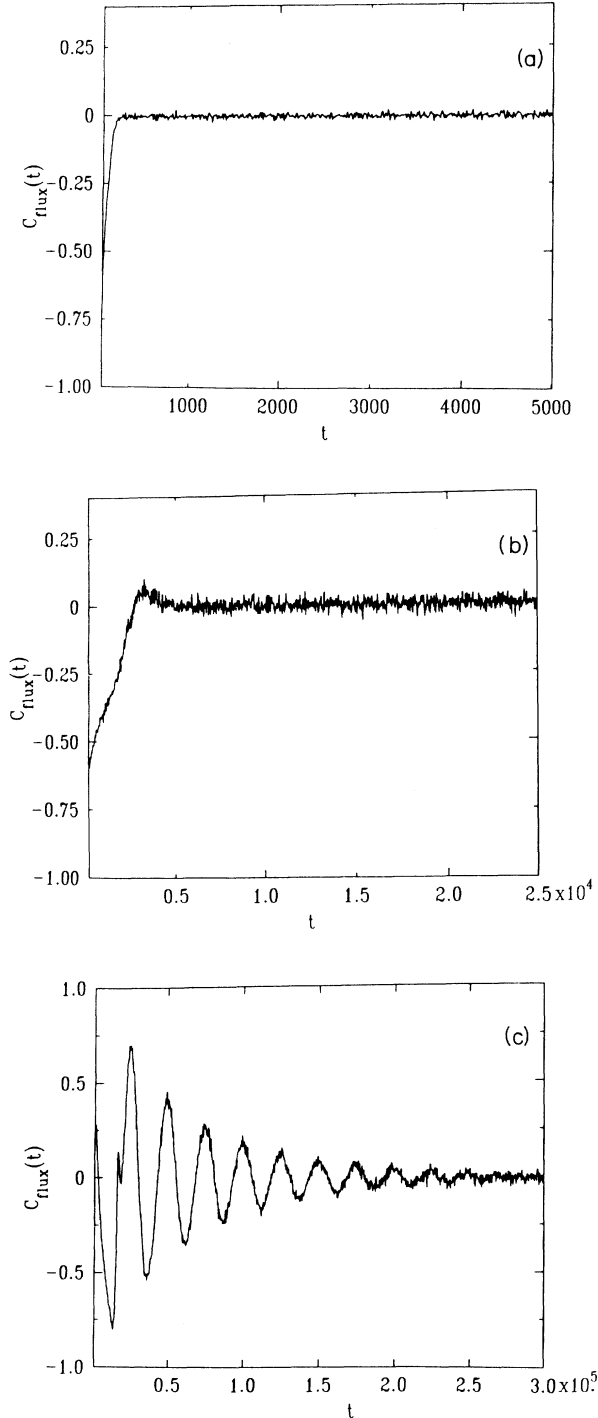


FIG. 6. Numerical results for the autocorrelation function of the mass flux in one dimension for the cases (a) $h_c = 2$ and (b) $h_c = 5$ for $L = 5000$, and (c) $h_c = 50$ and $L = 500$.

IV. AVALANCHES ON TWO-DIMENSIONAL SUBSTRATES

In two dimensions, the time until the first avalanche and the size of this initial avalanche can also be obtained by the statistical arguments given in Sec. II. For the initial avalanche to occur, the density must again reach a value where the most populated site contains h_c particles. Using the Poisson distribution, this condition is reached when a total of $L^{2(1-1/h_c)}$ particles have been deposited on the substrate. Consequently, the exponent $\alpha = 2(1-1/h_c)$ for a two-dimensional substrate.

An avalanche in two dimensions can accrete mass in the lateral as well as in the longitudinal direction. In the lattice model, stationary mass which is laterally nearest neighbor to the avalanche is defined to become part of the avalanche (Fig. 1). In the continuum case, any stationary droplet which is touched by the avalanche is considered to join the avalanche. Owing to this lateral mass accretion, the mass of the initial avalanche has a different dependence on system size than in one dimension. This size dependence can be found in terms of the shape of the region which is swept out by the avalanche. Since the first avalanche occurs when the density reaches a value of the order of L^{-2/h_c} , the cleared region will have a wedge shape whose opening angle α is given by $\tan(\alpha/2) \propto L^{-2/h_c}$. Multiplying the area of this wedge by the initial mass density leads to the mass of the initial avalanche scaling as $L^{\alpha'}$ with $\alpha' = (2-4/h_c)$. Analogous arguments yield the same values for the exponents α and α' in the two-dimensional continuum model.

We used numerical simulations to test many of these predictions. Figure 7 shows the distributions of mass added until an avalanche, $P(t)$, and the mass removed by an avalanche $R(m)$, for both the first avalanche, and in the steady state. These results were obtained from single-particle deposition on a square of linear dimension $L = 512$ for various thresholds h_c . Estimates for the exponents α and α' defined in Eqs. (7) were obtained by extrapolating simulation results for L in the range 32–512 to $L \rightarrow \infty$. Figure 8 shows the L dependence of the measured deviations of $\alpha(L)$ and $\alpha'(L)$ from their asymptotic values of $2(1-1/h_c)$ and $2(1-2/h_c)$, respectively. The behavior as $L \rightarrow \infty$ is in good agreement with our theoretical expectation.

A noteworthy feature of the distribution of initial avalanche sizes in two dimensions is the power-law behavior at small sizes, $R(m) \sim m^{-1/2}$, as shown in Fig. 7(b). This behavior stems from the fact that the location of the initial avalanche is uniformly distributed and that the size of the initial avalanche varies as the square of the distance from the bottom of the slope. Consequently, by first writing the size distribution as a function of the location of the avalanche and then changing variables from

avalanche location to avalanche size will lead to the power-law behavior observed in the figure.

Simulations were also performed for the off-lattice avalanche model. Figures 9 and 10 are “snapshots” of the system at various stages of evolution; these impart a

helpful visualization of the avalanche process. Immediately after the first avalanche, there is a characteristic wedge-shaped area that is cleared (Fig. 9). The steady-state configurations (Fig. 10) are relatively inhomogeneous and exhibit regions of large droplets which are just about to avalanche, as well as empty regions where avalanches have recently occurred. For these off-lattice simulations, the diameter of the deposited droplets was 1.5, and the substrate sizes ranged from 64×64 to 1024×1024 .

The shape of the cleared area can be found by a simple geometric argument (Fig. 11). When a moving droplet of mass m and radius $w \propto m^{1/D}$ falls a distance dy , it accretes additional mass dm which is proportional to the differential area swept out by the avalanche, $\rho w dy$, where ρ is the substrate mass density. This leads to a mass which increases with fall distance y as $(\rho y)^{D/(D-1)}$, or the width of the wedge growing as $(\rho y)^{1/(D-1)}$. For droplets of dimensionality $D=2$, the width of the wedge increases linearly with y , while for $D > 2$, the width grows more slowly.

In the off-lattice model, we also measured the distribution of mass added to initiate the first avalanche and the mass removed by the first avalanche. We considered both two- and three-dimensional droplets on a two-dimensional substrate. For droplets of spatial dimension $D=2$, the distributions shown in Fig. 12 are very similar, both qualitatively and quantitatively, to those of the lattice model on a two-dimensional substrate, as shown in Fig. 7. From the data for the average mass added to generate the first avalanche, M_a for $h_c = 3, 5,$ and 100 , we estimate the exponent α to be very close to our theoretical

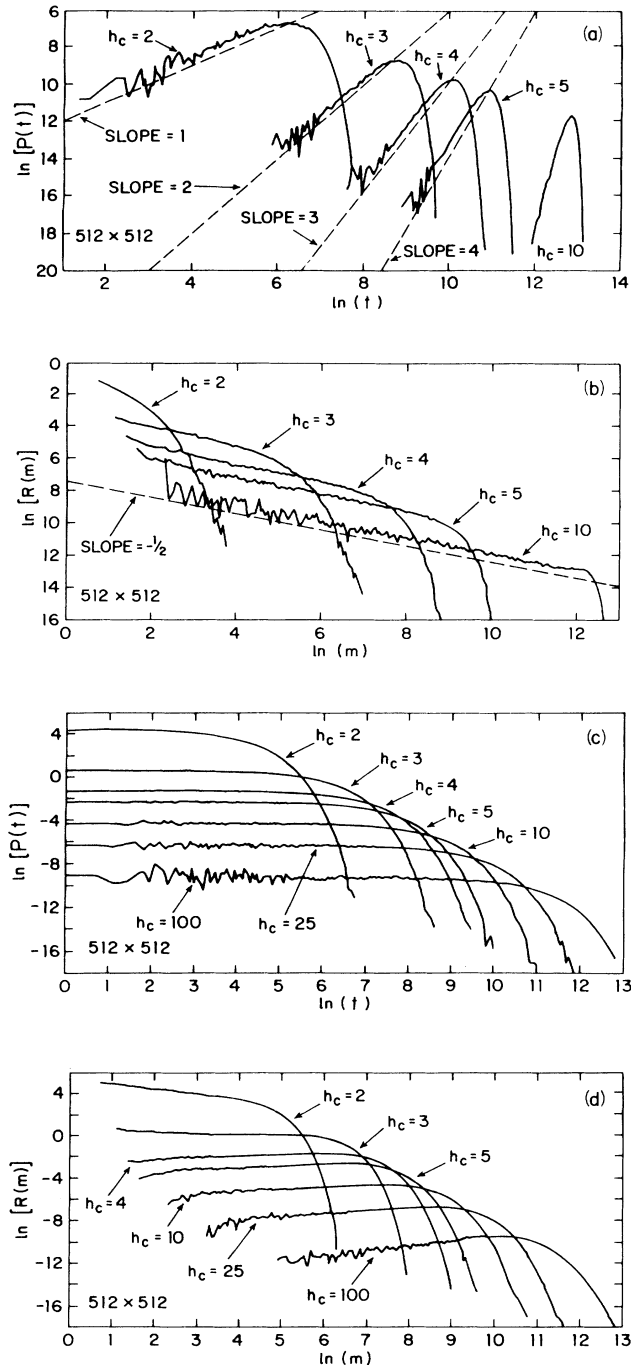


FIG. 7. Simulations results for the discrete avalanche model on a 512×512 substrate. Shown are (a) the distribution of times (or mass added) before the first avalanche and (b) the size distribution of the initial avalanche. In (c) and (d) the time and size distributions are shown in the steady state.

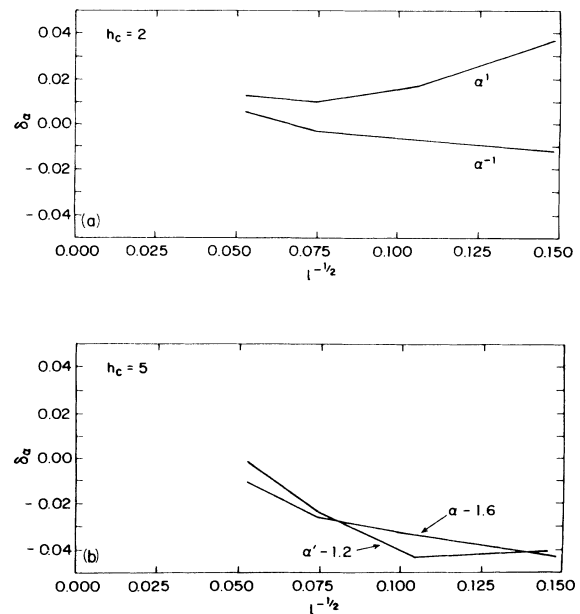


FIG. 8. Dependence of $\delta\alpha \equiv \alpha(L) - \alpha$ and $\delta\alpha' \equiv \alpha'(L) - \alpha'$ on lattice size L for (a) $h_c = 2$ and (b) $h_c = 5$. Here $\alpha = 2(1 - 1/h_c)$ and $\alpha' = 2(1 - 2/h_c)$.

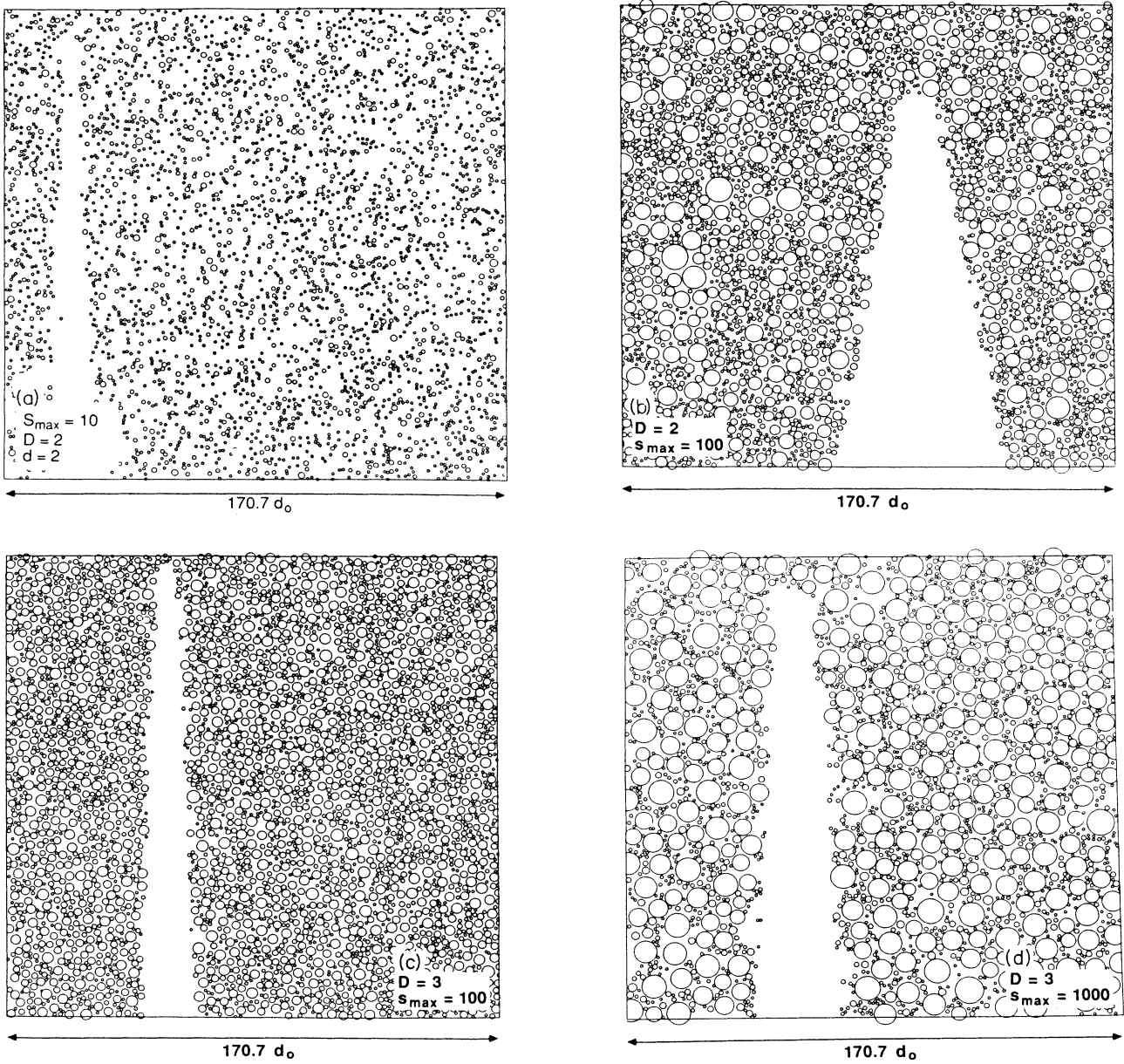


FIG. 9. “Snapshots” of two-dimensional off-lattice avalanche models just after the first avalanche has occurred for various values of D and h_c . The initial droplet diameter is 1.5 and the linear dimension of the system is 256.

prediction of $\alpha=1-1/h_c$ for both two- and three-dimensional droplets. However, for the exponent α' relatively large corrections to the asymptotic scaling behavior of $\alpha(L)$ on L exist. This appears to stem from the finite initial width $w_0 \sim h_c^{1/D}$ of the wedge swept out by the first avalanche.

This finite initial width of the wedge gives rise to a substantial contribution to the mass of an avalanche which is linear in y , in addition to the nonlinear contribution. To account for this linear component, we consider the quantity \mathcal{M}' :

$$\mathcal{M}' = \mathcal{M} - ah_c^{1/D} \rho L, \tag{27}$$

which is simply the mass of the avalanche with the linear contribution, whose amplitude is governed by an adjustable parameter a , subtracted out. By this analysis, the effective values of the exponent $\alpha'(L)$ were found to converge to a value close to $2-4/h_c$ as $L \rightarrow \infty$ for two-dimensional droplets.

For three-dimensional droplets, the fact that the region cleared by the avalanche has a width which grows more slowly than linear in the fall distance leads to qualitatively different predictions for the exponent α' . In this case, the area swept out by the initial avalanche scales as $\rho^{1/(D-1)} y_0^{D/(D-1)}$, where $y_0 \propto L$ is the distance from the

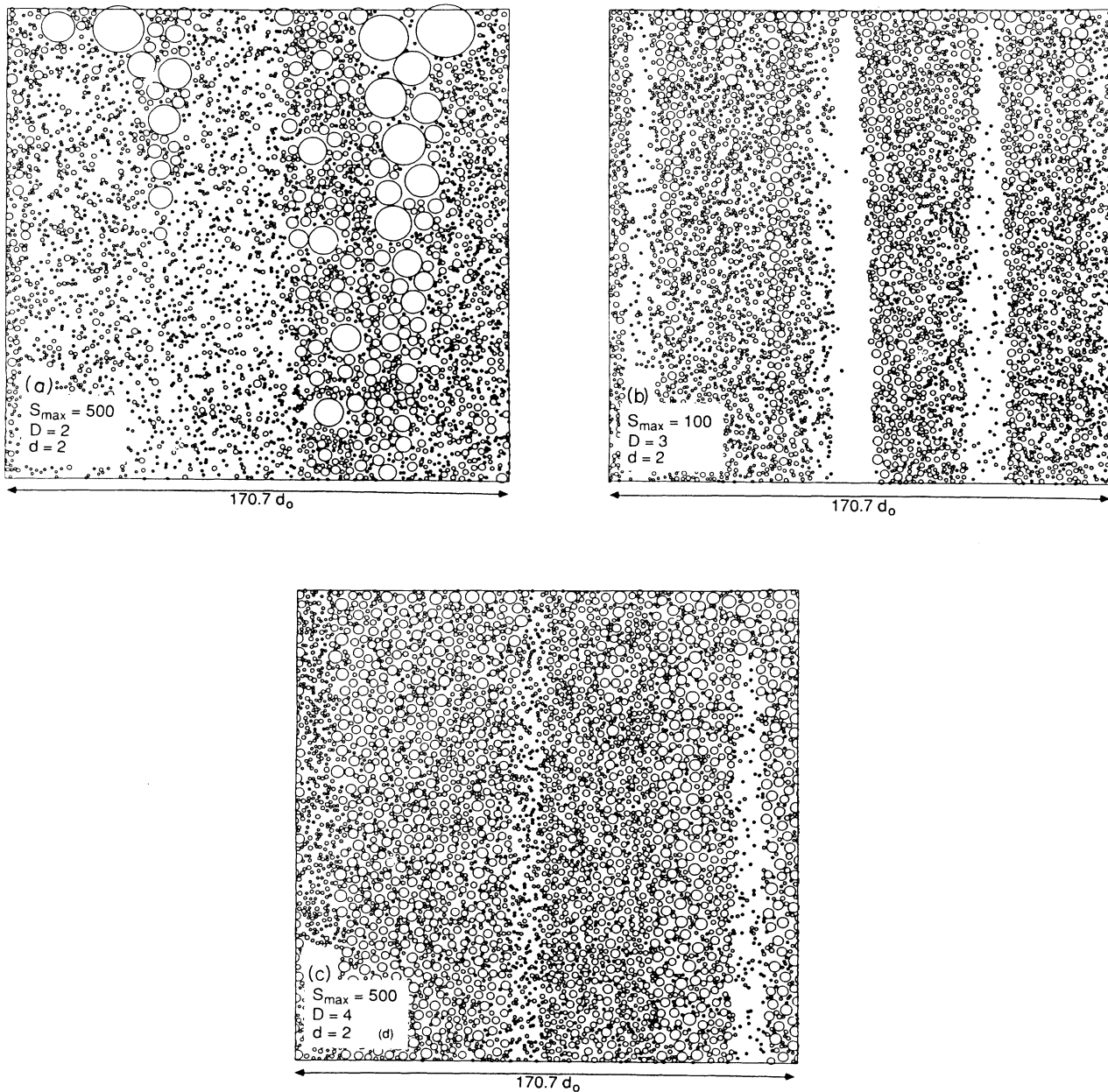


FIG. 10. Snapshots of the continuum system in the steady state for various values of D and h_c .

start of the avalanche to the bottom of the slope. Consequently, the mass in this cleared area scales as $(\rho L)^{D/(D-1)}$, and this leads to

$$\alpha' = \frac{D}{D-1} \left(1 - \frac{2}{h_c} \right). \quad (28)$$

Our numerical results for large h_c are in good agreement with this prediction (Fig. 13), but not so good for smaller values of h_c . Numerically, we find $\alpha' \approx 1.0$ and 0.45 , respectively, for $h_c = 5$ and 3 , while the corresponding values from Eq. (28) are 0.9 and 0.5 . In these cases, we

believe that the discrepancy stems from our simulations being too small to view the mass in the incoming path of the avalanche as a continuum.

V. DISCUSSION

We have introduced a simple avalanche model in which there is a continuous input of mass on a tilted substrate, with avalanches occurring whenever the mass at a given location reaches a preassigned threshold value. Inspired in part by the sandpile models of Bak and co-workers,^{1,2} one of the goals of our study is to ascertain

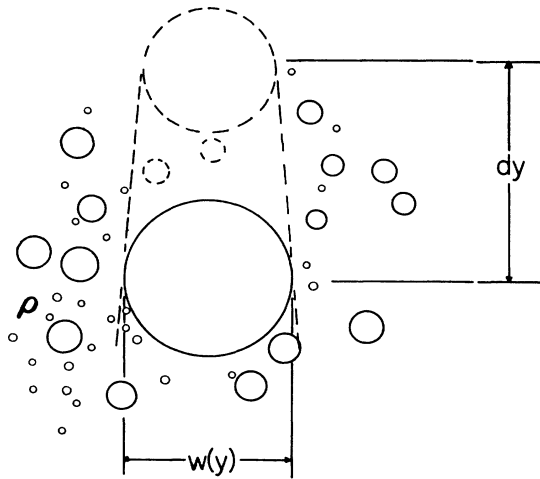


FIG. 11. Growth in the width of the cleared region as a droplet whose radius is proportional to $m^{1/D}$ falls a distance dy . The mass within the region swept out by the falling droplet $\rho w dy$ contributes to the increase in the droplet mass.

the type of dynamical behavior that can occur in open systems for which transport is inhibited by an intrinsic threshold. We anticipate that experimental studies of this system will provide the impetus for additional theoretical work.

A basic feature of our model is that once an avalanche

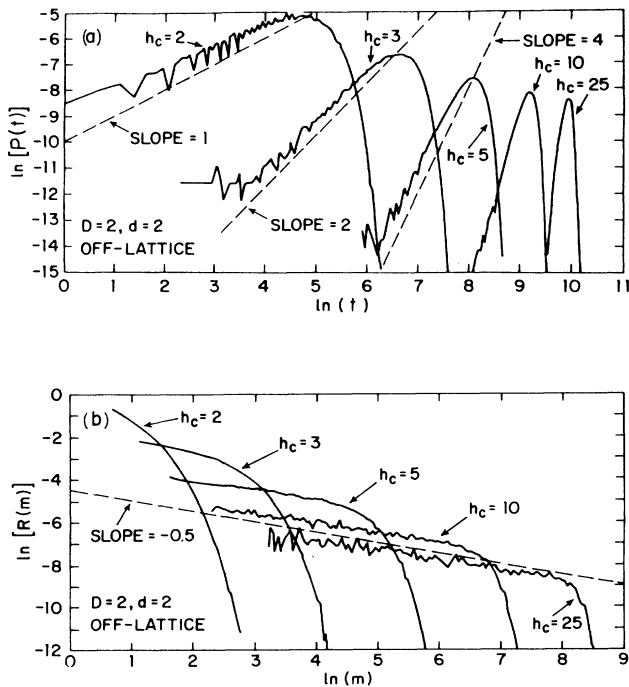


FIG. 12. Distribution of (a) the times until the first avalanche $P(t)$, and (b) the mass removed by the first avalanche, $R(m)$, obtained from off-lattice simulations of two-dimensional ($D=2$) droplets for several values of h_c .

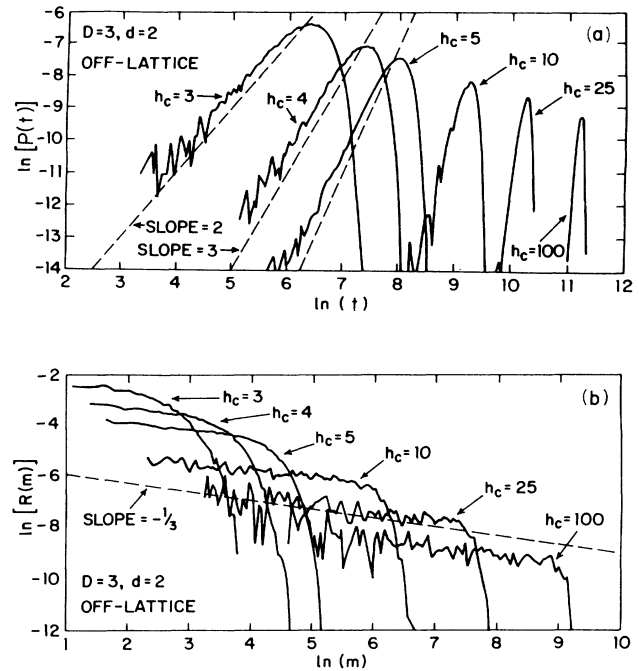


FIG. 13. A plot similar to Fig. 12, except for three-dimensional droplets ($D=3$).

starts, it necessarily propagates instantaneously to the end of the system. Thus our model is dominated by inertial effects, whereas the self-organized criticality models of Bak and co-workers are strongly dissipative in nature. This seems to be an essential reason for why power-law decays in the autocorrelation functions associated with mass transport do not arise in our avalanche model. Experimentally, it is not obvious how to design a system which will be dominated by dissipation. In the two recent experiments on real sandpiles,^{6,7} the systems have to be driven a finite "distance" from the critical state in order to generate mass transport. In this aspect, the experiment of Jaeger, Liu, and Nagel exhibits several features which are qualitatively similar to our model. Because the system must be driven by a finite amount to generate avalanches, there is a characteristic relaxation time which is related in some fashion to this driving distance. However, in the sandpile experiment it seems that the avalanche involves the entire surface, as the slope is described always by a single angle. This would correspond to the maximal avalanches that occur in our model. It might be interesting to perform sandpile experiments in much larger systems, so that size-dependent effects, similar to what we observe, might be studied. Furthermore, large sizes might allow one to observe the dissipation that could give rise to power-law dynamical behaviors.

While inertial effects appear to play a primary role in governing the avalanche dynamics in our model, it is evident that in an experimental realization of water drops sliding down an inclined plane, an avalanche is not necessarily catastrophic nor is it instantaneous. Owing to wet-

ting effects, a sliding drop may leave behind a trail of liquid, and this mass loss can eventually cause the droplet to stop. This stopping mechanism appears to be analogous to the dissipation in the sandpile models. Consequently, by generalizing our model to allow for the possibility that an avalanche can lose mass and also can stop when a lower mass threshold is reached, one might recover some of the scaling properties of the sandpile model. It should therefore be interesting to study experimentally the dynamics of liquid droplets sliding down both wetting and nonwetting substrates.

For our avalanche model, the dynamical behavior depends crucially on the ratio of the threshold h_c to the logarithm of the system size L (in one dimension). For small thresholds, the cleared region downhill from the avalanche can quickly fill up to the avalanche threshold again. Consequently, the location and size of successive avalanches is essentially uncorrelated. For large thresholds, a relatively predictable sequence is followed. There is a long quiescent period where mass builds up to the threshold height on the substrate. Then there follows a short period of intense activity in which each avalanche breaks off uphill from the previous event. This phase ends when an avalanche begins at the top of the slope, thus sweeping the system clean. In the case where $L \rightarrow \infty$, it is possible to formulate a continuum approach that pre-

dicts the system size and threshold dependence of many dynamical quantities.

There are several additional aspects of the avalanche model which could be modified in order to explore the influence of such variations on the dynamics of the system. These include allowing for a finite propagation time for an avalanche, and also allowing for an incomplete sweeping away of the already-deposited mass as the avalanche passes by. By varying the parameters associated with these generalizations, one might gain a better understanding of underlying mechanisms of the power-law decay of correlations in the sandpile models. These generalizations may also prove to be useful in interpreting experimental systems of fluid drops sliding down inclined substrates.

ACKNOWLEDGMENTS

We thank D. ben-Avraham, P. Bak, and C. L. Henley for helpful discussions. This work was supported in part by the U.S. Army Research Office (Boston University), and by the Office of Naval Research and the Petroleum Research Fund Administered by the American Chemical Society (Emory University). This financial assistance is gratefully acknowledged.

-
- ¹P. Bak, C. Tang, and K. Wiesenfeld, *Phys. Rev. Lett.* **59**, 381 (1987); *Phys. Rev. A* **38**, 364 (1988).
²C. Tang and P. Bak, *Phys. Rev. Lett.* **60**, 2347 (1988); *J. Stat. Phys.* **51**, 797 (1988).
³T. Hwa and M. Kardar, *Phys. Rev. Lett.* **62**, 1818 (1989).
⁴L. P. Kadanoff, S. R. Nagel, L. Wu, and S.-m. Zhou, *Phys. Rev. A* **39**, 6524 (1989).
⁵J. Souletie, *J. Phys. (Paris)* **44**, 1095 (1983).
⁶H. M. Jaeger, C. Liu, and S. R. Nagel, *Phys. Rev. Lett.* **62**, 40 (1989).
⁷P. Evesque and J. Rajchenbach, *Phys. Rev. Lett.* **62**, 44 (1989).
⁸B. Lewis and J. C. Anderson, *Nucleation and Growth of Thin*

- Films* (Academic, New York, 1978).
⁹F. Family and P. Meakin, *Phys. Rev. Lett.* **61**, 428 (1988).
¹⁰D. Beysens and C. M. Knobler, *Phys. Rev. Lett.* **57**, 1433 (1986).
¹¹J. L. Viovy, D. Beysens, and C. M. Knobler, *Phys. Rev. A* **37**, 4965 (1988).
¹²B. J. Mason, *The Physics of Clouds* (Oxford University Press, London, 1957).
¹³P. Meakin and F. Family (unpublished).
¹⁴See, e.g., Z. Cheng and S. Redner, *Phys. Rev. Lett.* **60**, 2450 (1988).
¹⁵T. Vicsek and F. Family, *Phys. Rev. Lett.* **52**, 1669 (1984).